MOLD POWDERS CHARACTERIZATION USING SEVERAL DIFFERENT METHODS

P. H. S. CARDOSO, L. ROLDO, C. A. M. MORAES, P. R. LEAL, T. B. KASPARY, T. R. STROHAECKER and A. C. F. VILELA

Universidade Federal do Rio Grande do Sul - Escola de Engenharia – PPGEM
Av. Osvaldo Aranha, 99 Sala 613. CEP: 90035-190, Porto Alegre, RS – Brazil.

Abstract: In order to optimize the application of mold powders which are used in continuous casting processes of steelmaking, several chemical and structural analysis techniques were employed to characterize their components. Three different powders were analyzed in three different conditions. Such conditions were:

1. The as-received powder (collected in the steel mill before use);
2. Dried powder at 120°C for 24 hours;
3. Melted in a graphite crucible via a laboratory furnace.

Due to the complexity of the mold powder characterization, XRD (X-ray Diffraction), Micro Raman Spectroscopy, EDX (Energy Dispersive X-ray) and X-ray Fluorescence techniques were carried out to fully investigate the material. TG (Thermogravimetry) was also used to determinate the behavior of the powder under heating. A very good qualitative phase composition was obtained for each sample condition. Wollastonite (calcium silicate) was the major phase found between the as-received powders, and between the molten powders the encountered major phase was cuspidine.

Key words: Mold powders, Continuous casting, Raman spectroscopy, XRD, TG.

---

1. INTRODUCTION

It has been found that, in the last few years, mold powders have had significant implication in continuous casting technology due to the big improvement of the steel quality.

The determination of mold powders chemical and structural characteristics play an important role in the efficiency of the continuous casting process and also in the steel quality.

The variability in the characteristics causes much concern in selecting and using mold powders since the correct powder is essential to successful casting. An inappropriate selection can lead to tremendous liabilities associated with safety, equipment, damage, loss of productivity and unfavorable customer perception[1)]. In this way, it is important to have a clear understanding about the exact role mold powder plays.

Mold powders or mold fluxes are synthetic slags used to cover the liquid pool surface during the continuous casting of steel[2)].

Kashiwaya et al. says that various studies have shown that the slag film formed between mold and strand contains three layers: a glassy zone close to the mold, a crystalline layer in the center and a liquid film in contact with the steel[3)].

The basic functions of mold powders are[4)]:

- Provide lubrication between the strand and the mold;
- Moderate heat transfer between the mold and the strand;

- Prevent reoxidation;
- Provide thermal insulation;
- Act as reservoir for the absorption of inclusions, both solid and liquid, from the liquid steel.

In general, inappropriate mold powder application can result in[4]:

- Surface cracking;
- Sub-surface cleanliness problem on the castings;
- Slag patches on the surface of continuous cast sections;
- Chemical interaction between the liquid steel and the liquid mold flux;
- Environmental problems due to fluxes that are unstable at high temperatures and release fluorine containing gases to the atmosphere or become dissolved into the water system below the mold accelerating corrosion of the structural components.

In terms of conventional chemical analysis, the main components[5, 6] usually present in mold powders are quartz (SiO_2), lime (CaO), sodium oxide (Na_2O), fluorspar - fluorite (CaF_2), and carbon (C). Other components[5, 6] that eventually appear in reasonable amounts are alumina (Al_2O_3)[5], burnt magnesite (MgO)[5], some alkaline oxides (K_2O, LiO_2), and some metal oxides (iron, manganese, titanium)[6]. At the same time, the X-ray diffraction analysis has shown that many of these components are present as more complex phases, e.g., wollastonite ($CaSiO_3$)[7], limestone ($CaCO_3$), sodium carbonate (Na_2CO_3), sodium fluoride (NaF), and cuspidine ($Ca_4Si_2O_7F_2$)[7] in the melted flux, for example. Such complexity can be easily seen in the case of carbon, which may be added to the powder as coke dust, lamp black, graphite, or fly-ash, or even be present as calcium and sodium carbonate[6]. Those findings have brought the need to characterize these fluxes by using several different techniques.

The results obtained by employing XRD, Micro Raman Spectroscopy, EDX, X-ray Fluorescence and TG techniques will be shown and discussed with the purpose of helping to understand the complexity of the mold powders components action.

2. EXPERIMENTAL

2.1 Material

Three different powders **I**, **J** and **K** were analyzed in three different conditions. Such conditions were:

1. The as-received powder (collected in the storage bin);
2. Dried powder at 120°C for 24 hours;
3. Twenty grams of powder were melted in a graphite crucible using a laboratory electric induction furnace at 1500°C for 30 minutes plus 2 hours of soaking time and cooled inside the furnace.

Every powder was crushed in an alumina crucible and sifted with a 100-mesh screen before any analysis.

2.2 Experimental Details

Experiments, to each powder, were carried out using:

1. X-ray Fluorescence: This technique was carried out in a Philips PW-2600, utilizing a standard pattern.
2. Energy Dispersive X-ray (EDX): The EDX analysis were carried out in a Philips SEM/EDAX microprobe. The acceleration voltage employed was 20 KeV. By this way problems of light elements over voltage were avoided.
3. X-ray Diffraction (XRD): The X-ray patterns were recorded by Philips X'Pert MPD X-ray Diffractomer with Cu$k\alpha$ radiation of 1,54056nm. The measuring parameters were settled as follow. The time, per each step of 0,02 degrees, was 4 seconds. Spinning speed (when employed) was 1 rev/s.
4. Micro-Raman Spectroscopy: Raman spectra were collected in the wavenumber range of 100-1700 cm^{-1} with a laser micro-Raman setup (Dilor LabRam, ISA Jobin-Yvon) that was coupled to an optical microscope (Olympus BX40). Red light, (wavelength, λ, of 632.817nm) from a HeNe 20 mW laser. Gratings of 1800 grooves/mm and laser filter monochromator were used. The laser is focused onto the sample through a 50X and 100X objective. The Raman signal was directed into a thermoelectrically cooled CCD two-dimensional image detector system.
5. Thermogravimetry analysis (TG): The thermogravimetric analysis was carried out using a NETZSCH STA 409C Thermal Analysis Apparatus. A platinum-iridium crucible containing 0,100g of powder was heated up to 1450°C under an oxidizing atmosphere by pouring 200 ml of air. The heating and cooling rates were 10°C/min.

3. RESULTS and DISCUSSION

Tables 1A and 1B present the X-ray fluorescence chemical analysis results for each powder in the as-received and melted condition, respectively. Results are presented in oxides form, however, the carbon values are not totally trustable because of carbon can be burned during the sample drying step.

The basicity (relation CaO/SiO_2), considering the above analysis, was calculated as 0,9; 0,66 and 1,03 (table 1A); and 0,71; 1,06; 0,96 (table 1B) for powders I, J and K, respectively.

Tables 2A and 2B present EDX results for the containing elements in each powder from the as-received and melted condition, respectively.

Tables 3A and 3B present the EDX results in an oxide quantification form. The values of C and F are in elemental form because the software is not able to give the most probable components that contain those elements. Those components could be $(Na_2, Ca)CO_3$ and CaF_2, respectively.

A reasonable quantitative relationship was not obtained between both techniques, so any comparison between them was not possible.

The quantitative correlation between as-received and melted condition in the same technique was not verified either. Both EDX and fluorescence are in agreement in the tendency of increasing the amounts of the three main components (CaO, SiO_2 and Al_2O_3) from the as received to the melted condition.

The Na_2O and C amounts, even not trustable as absolute values, present a tendency of decreasing from the as received to the melted condition. On the other hand, The F amount of the EDX presents the same increasing tendency of Ca, Si and Al. In this way, comparing both techniques, and considering the oxides form, it is necessary to require the same components in the final result. It means that if FeO, for instance, is required at fluorescence one can not ask for Fe_2O_3 in EDX.

Both techniques should be used only as indicative of powder composition. Over voltage problems in EDX can also lead to errors in the measurements.

Viscosity characteristics of the powders that can be determined by a basicity ratio (CaO/SiO_2) can be trustable using both techniques due to the same tendency of increasing and decreasing values. There is a tendency in decreasing the basicity of the melted, even without any interaction with liquid steel. As the basicity values are quite different the viscosity and the capacity to absorb inclusions can be affected. As a result of this observation, it can imply that the melted powder have different properties from those encountered in the as-received powder.

Even though, The chemical analysis results has raised some doubts, in the industry, the most common technique[8)] to determine the chemical analysis of mold powder is fluorescence, because the sample preparation and the equipment are easy and fast tools.

Figures 1, 2 and 3 presents the X ray diffraction patterns in the unmelted condition for powder I.

The results shown in figure 1 are from as received powder. It was observed that the relative intensities of the phases were not in agreement with those for JCPDS patterns. Several peaks from important phases presented very high intensity in 2θ in which, according to JCPDS, the intensities were supposed to be very low. This feature is related to the absence of homogeneity in the powders, i.e., some grains from a specific phase could be in a favorable orientation according to the diffraction axes, and by this way his intensity very higher than expected.

In figure 2 the same powder was submitted to a drying process. The purpose for this step was to avoid wrong phases identification in function of hydrate phases. The phase result was the same, but some peaks decreased and some others increased its relative intensity. This fact confirms the powder non-uniformity.

The next step was to implement the diffraction using spinning in the sample holder. By this way the area submitted to the X ray changed during the analysis and this non-uniformity should be avoided.

In figure 3 the X ray diffraction of the as received powder, non dried, with spinning is showed. In fact, in this pattern, the intensities were not in complete agreement with those from JCPDS. The resultant area generated by the Lorentz and Gauss fitting gave a good explanation for peaks overlapping. Even though quantitative analysis were not performed in function of too many phases present.

In powder I the mainly encountered phases are in agreement with the indicative results obtained in Fluorescence and in EDX. These phases are **(1)** $CaSiO_3$ (wollastonite), **(2)** SiO_2 (quartz), **(3)** CaF_2 (fluorite), **(4)** $CaCO_3$ (calcium carbonate) and **(5)** Na_2CO_3 (nitrite).

The same approach was employed to the other two powders (J and K).

Figures 4, 5 and 6 are from powder J and they are presented in same sequence of analysis. The encountered phases were the same from powder added of **(6)**. $NaSiF_6$

(malladrite), **(7)**. $CaSO_4$ (calcium sulfide).Figures 7, 8 and 9 are from powder K and they also are presented in the same sequence. The phases in powder K are the same from powder J.

It is useful to say here that the wollastonite presented belongs to a monoclinic system. This in because this phase was in the best agreement with the X ray pattern. According to literature [9], the most common wollastonite phase is triclinic. The JCPDS pattern for this phase was also a good pattern. In the case of the powders I, J and K it is possible that this phase is present. Or even that both phases are present in the powders. In this paper the choice was for the monoclinic phase.

Wollastonite seems to be the phase present in the higher amount. For this phase a preferential X ray diffraction orientation was found in the direction (200). Fluorite seems to be very favorable to X ray diffraction. In the chemical analysis the F level was not as big as necessary for such diffraction intensity (fig. 1, phase 3, hkl 111). This phase was identified as a cubic system.

In each diffraction pattern (fig. 1-9) indicatives of amorphous phase were found. This Phase probably belongs to Aluminum or even Silicon.

Figures 10, 11 and 12 present X ray diffraction for the melted powders I, J and K respectively. The mainly component was cuspidine ($Ca_4Si_2O_7F_2$). Some phases from the original diffraction (unmelted state) were maintained (CaF2, SiO2 and Na2O). Some indicative of amorphous phase was also found, but in one case a phase containing Aluminum was found ($CaAl_2SiO_2$). Some peaks were unidentified and may be that using spinning in function of non-uniformity this phase could be found in the other cases.

Concerning Micro Raman it is pointed that:

Due to the heterogeneity of the powders, different regions of the same sample were analyzed and called as Powder I1, I2 and I3, for example, (figures 13 – 18).

According to the Raman of the pure phases (figure 19), it was observed that in Raman spectra of powder I, J and K, as-received condition, wollastonite, SiO_2, CaF_2, $CaCO_3$ and hydrated Na_2CO_3 are present. However in Raman spectra of powder I, J and K, melted condition, the peaks position were not the same, that gives idea of presence of cuspidine.

It was not possible in this paper to find a Micro Raman pattern from cuspidine[10], and also was not possible to get pure cuspidine to make our own pattern as in pure phases from the unmelted condition (paragraph above).

The pure phases for Raman were confirmed as pure ones either by X ray diffraction (figures 20-24) and by comparison with database[10].

The thermogravimetric analysis of the powders I, J and K (figure 20) implies, by the mass loss of both powders, the tendency of the C and Na amounts decreasing pointed out earlier in the discussion. The mass loss observed in all samples indicates that elements or compounds can be, essentially, volatilized at temperatures in the range of 400 to 800°C. It is known that $CaCO_3$ decomposes in a temperature range specified above. As a result of that C was probably carried out from the powder as CO_2. In the case of Na, it is known that this element volatilizes at 885°C, so the lower amount encountered in the melted powders suggest its volatilization. TG analysis also shows that sample K is the one with the lowest amount of C (tables 1A and 3A), resulting in the lowest mass loss between the powders during the heating up till 1450°C. This result can be confirmed by the X-Ray diffraction of powder K (figures 7-9, hkl 104, IR = 100%) which showed a very low presence of $CaCO_3$.

4. CONCLUSIONS

Na and C seem to be the main components that volatilize at low temperatures according to chemical analysis, and TG.

The chemical analysis either by fluorescence or by EDX have some discrepancy , as a result of this they were used as indicative techniques.

A good complementary agreement was encountered between the technique X-ray diffraction and Raman.

The results from TG are in agreement with x ray diffraction analysis.

Wollastonite was the major phase encountered in the as received powder and cuspidine in the melted one.

REFERENCES

1) Branion, R.V.; Dukelow, D. A.; Lawson, G. D.; Schade, J.; Schmidt, M.; Tsai, H. T. Standardized Testing of Mold Powder Properties. Steelmaking Proceedings, (1995), pp. 647-653.
2) Chávez, J. F.; Rodríguez, A.; Morales, R.; Tapia V. Laboratory and Plant Studies on Thermal Properties of Mold Powders. Steelmaking Proceedings, (1995), pp. 679-6686.
3) Kashiwaya, Y.; Cicutti, C. E.; Cramb, A. W. An Investigation of the Crystallization of a Continuous Casting Mold Slag Using the Single Hot Thermocouple Technique. ISIJ International, Vol. 38, (1998), No 4, pp. 357-365.
4) Feldbauer, S.; Jimbo, I.; Sharan, A.; Shimizu, K.; King, W.; Stepanek, J.; Harman, J.; Cramb, A. W. Physical Properties of Mold Slags that are Relevant to Clean Steel Manufacture. Steelmaking Proceedings, (1995), pp. 655-667.
5) Wingrove, J. Identification of Iron Oxides. Journal of The Iron and Steel Institute, (1970), pp. 258-264.
6) Stoffel, H.; Fischer, H.; Schulz, K. Case Study: use of the Differential Thermal Analysis (DTA) for Selective Carbon-loss in Casting Powder Mixtures. 12th IAS Steelmaking Seminar Proceedings, 1999, pp. 429-438.
7) Cicutti, C.; Cramb, A.; Kashiwaya, Y. Study of crystallization in mold slags. Continuous Casting Course, IAS, San Nicola, Argentina, june, 1999.
8) Frazee, M. J. Status Report: ASTM Comitee CO8.11 Standardization work on Metallurgical Powders. Steelmaking Conference Proceedings, USA, 1995, pp. 639-653.
9) Swamy, V.; Dubrovinsky, L. S.; Tutti, F. High-Temperature Raman Spectra and Thermal Expansion of Wollastonite. Journal of the American Ceramic Society, Vol. 80, (1997), No 9, pp. 2237-2247.
10) Nyquist, R.A.; Putzig, C.L.; Leugers, M.A. Infrared and Raman Spectral Atlas of Inorganic Compounds and Organic Salts, Vol. 1-4.

ACKNOWLEDGEMENTS

The authors are grateful for the sponsoring from the FINEP-PADCT to the research project, and CNPq and CAPES for sponsoring the research assistants, agencies from the Brazilian Federal Governments.

1. Presentation of X-ray Fluorescence Results

Table 1A - Chemical analysis of as-received mold powders (wt%).

	CaO	SiO_2	MgO	Al_2O_3	FeO	MnO	Na_2O	K_2O	C	Cr_2O_3	TiO_2
Powder I	28,90	32,00	2,60	5,58	2,83	0,14	7,23	0,85	18,00	0,22	0,49
Powder J	26,50	40,18	1,49	3,55	1,58	0,14	4,76	0,16	20,00	0,23	0,28
Powder K	37,90	36,7	0,8	3,3	0,9	0,08	7,20	0,13	3,6	0,15	0,1

Table 1B – Chemical analysis of melted mold powders (wt%).

	CaO	SiO_2	MgO	Al_2O_3	FeO	MnO	Na_2O	K_2O	C	Cr_2O_3	TiO_2
Powder I	32,5	45,5	2,95	8,30	1,66	0,10	2,22	0,39	0,15	0,15	0,42
Powder J	42,78	40	1,75	8,36	1,22	0,11	0,94	0,11	0,05	0,18	0,30
Powder K	40,12	41,62	1,32	5,54	0,97	0,09	1,88	0,06	0	0,14	0,10

2. Presentation of EDX Results

Table 2A – Chemical analysis of as-received mold powders (wt%).

	Ca	Si	Mg	Al	Fe	S	Na	K	C	F	O
Powder I	9,03	6,88	0,52	1,56	1,05	0,26	13,69	0,51	34,18	1,67	30,64
Powder J	13,17	5,87	-	1,32	0,57	0,24	7,27	-	43,15	1,27	27,15
Powder K	15,88	11,81	-	1,28	0,74	-	12,39	-	22,94	3,14	31,81

Table 2B – Chemical analysis of melted mold powders (wt%).

	Ca	Si	Mg	Al	Fe	S	Na	K	C	F	O
Powder I	19,13	17,94	1,37	3,53	1,13	0,44	4,13	0,28	11,19	4,74	36,13
Powder J	20,26	11,58	0,55	2,96	0,58	0,23	0,50	-	31,08	3,72	28,53
Powder K	20,54	20,29	0,71	3,58	0,42	-	4,74	-	6,74	6,11	36,85

3. Presentation of EDX Results quantified by oxides

Table 3A – Chemical analysis of as-received mold powders (wt%).

	CaO	SiO_2	MgO	Al_2O_3	Fe_2O_3	Na_2O	K_2O	C	F
Powder I	14,57	19,61	1,14	3,91	1,64	20,94	0,72	34,18	3,29
Powder J	21,04	16,98	-	3,39	0,89	11,82	-	43,15	2,73
Powder K	22,93	28,13	-	2,71	1,06	17,5	-	22,94	4,73

Table 3B – Chemical analysis of melted mold powders (wt%).

	CaO	SiO_2	MgO	Al_2O_3	Fe_2O_3	Na_2O	K_2O	C	F
Powder I	26,06	38,53	2,28	6,7	1,56	5,56	0,33	11,19	7,79
Powder J	28,27	26,95	1,00	6,01	0,81	0,71		31,08	5,55
Powder K	27,66	42,53	1,16	6,62	0,57	6,24	-	6,75	8,47

4. XRD Results for the unmelted powders

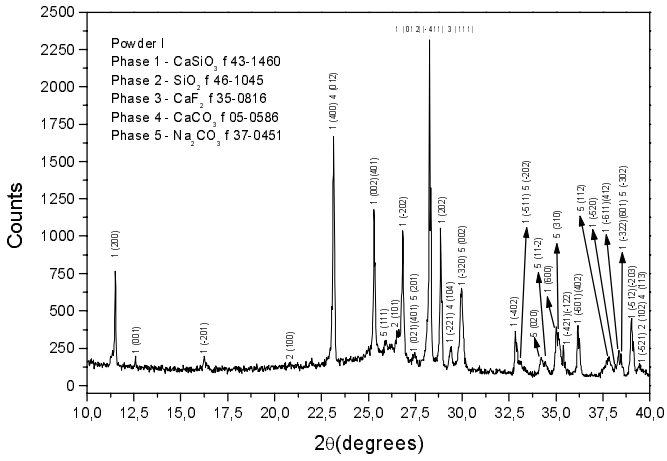

Figure 1 –XRD of the as received powder I

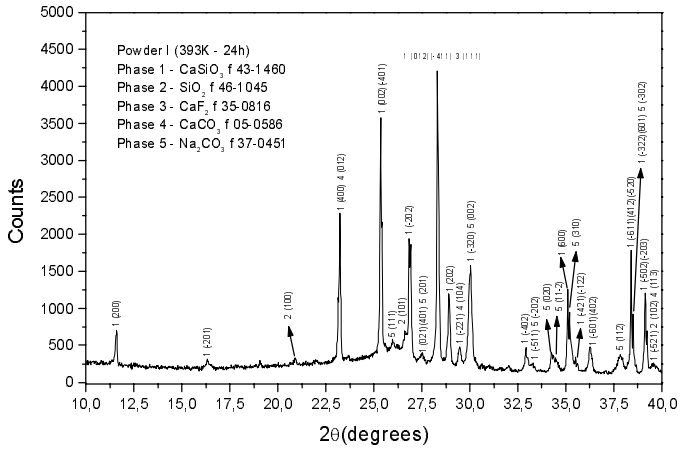

Figure 2 – XRD of the dried powder I

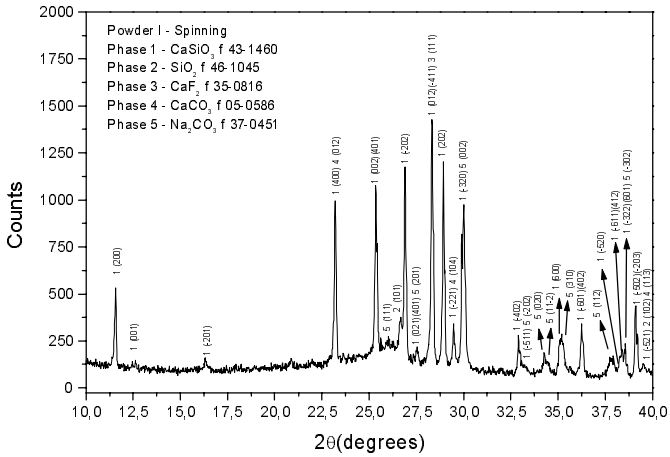

Figure 3 – XRD of the spinned powder I

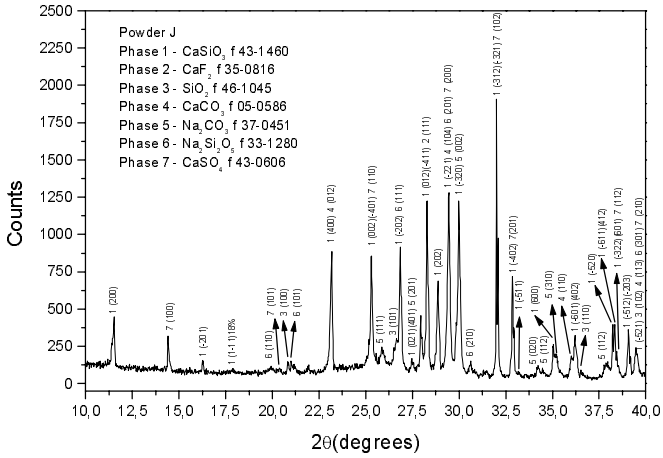

Figure 4 –XRD of the as received powder J

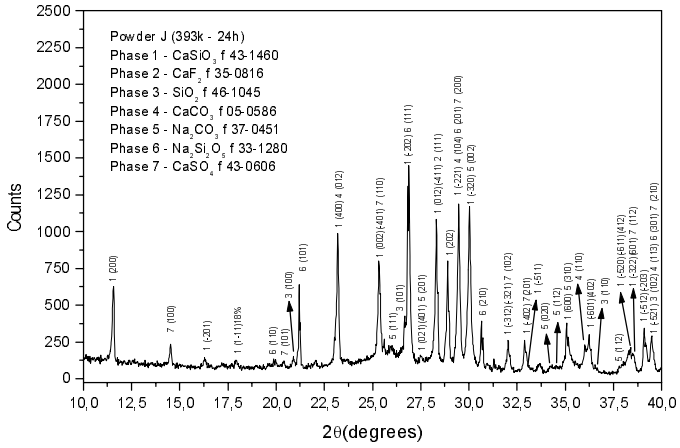

Figure 5 – XRD of the dried powder J

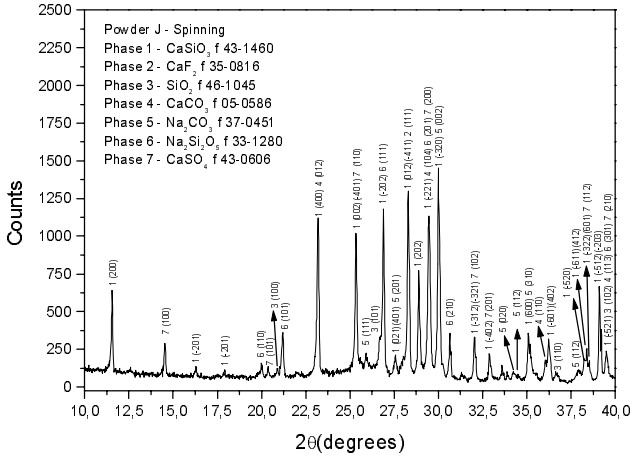

Figure 6 – XRD of the spinned powder I

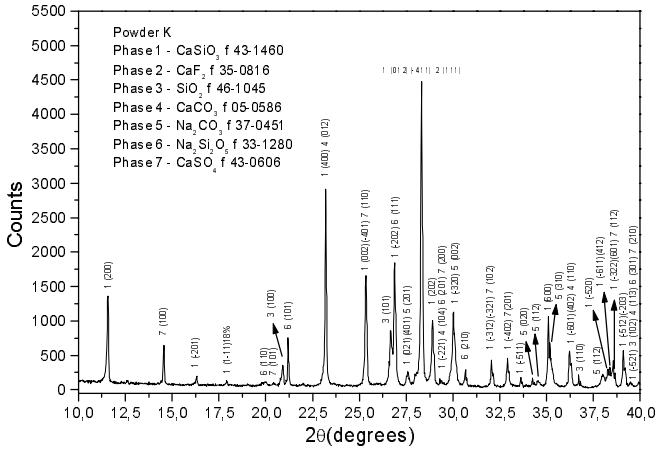

Figure 7 –as received powder K

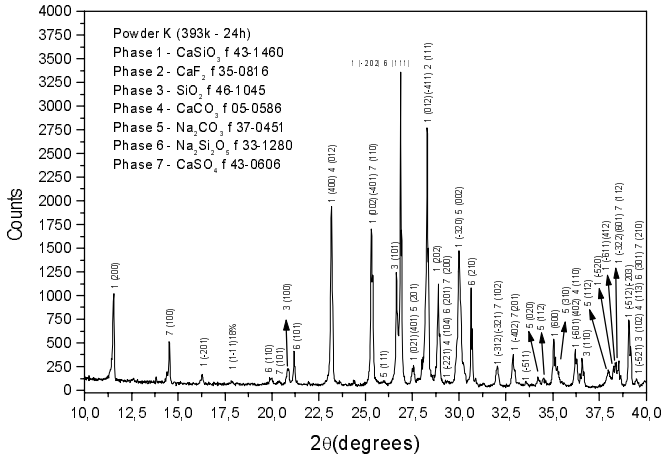

Figure 8 – XRD of the dried powder K

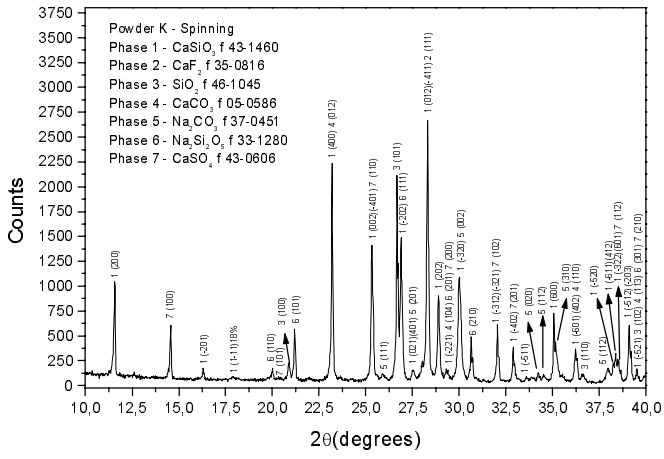

Figure 9 – XRD of the spinned powder K

5. XRD Results for the melted powders

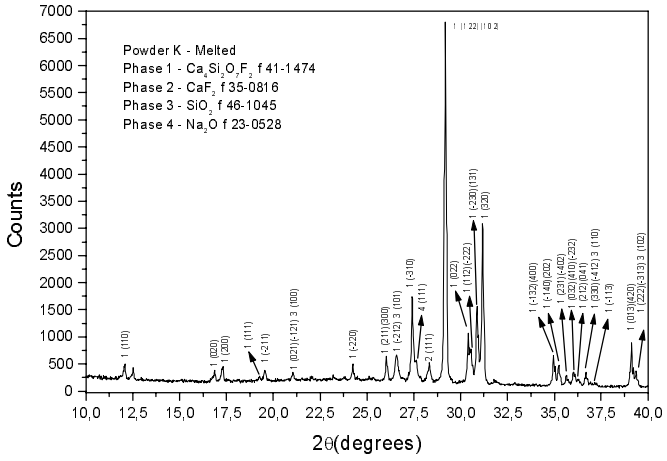

Figure 10 – XRD of the melted powder K

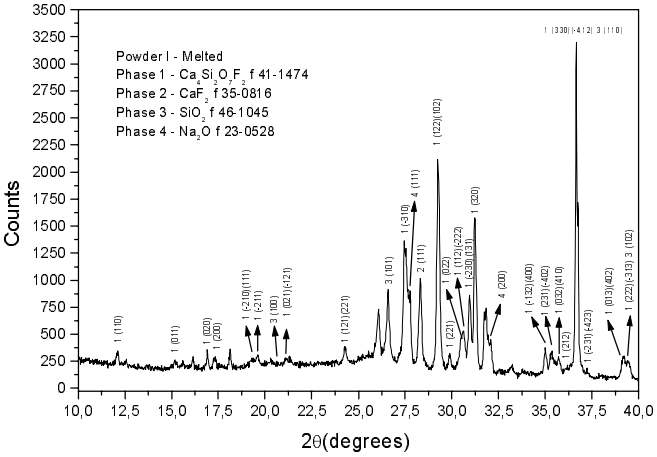

Figure 11 – XRD of the melted powder I

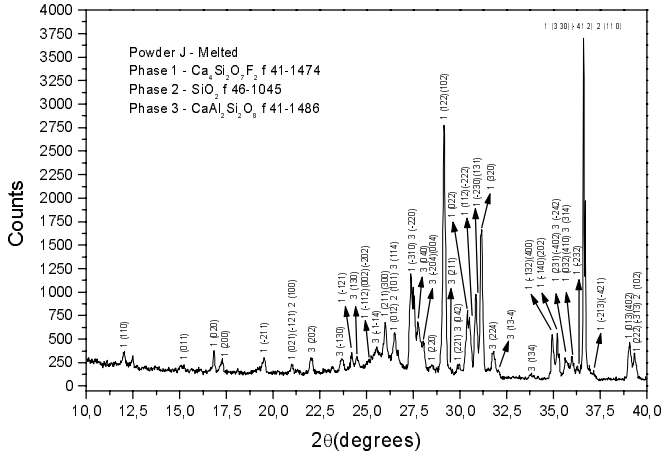

Figure 12 – XRD of the melted powder I

6. Presentation of micro-Raman Results

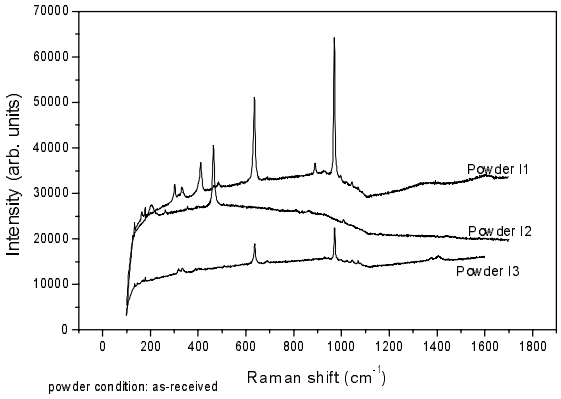

Figure 13 – Raman of powder I (as-received)

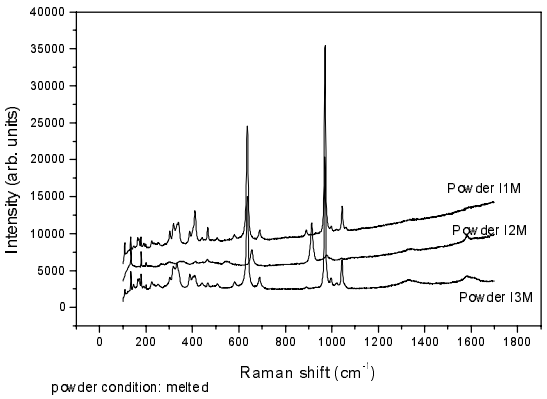

Figure 14 – Raman of powder I (melted)

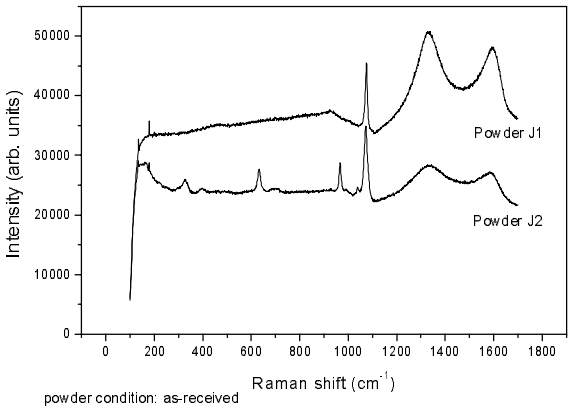

Figure 15 – Raman of powder J (as-received)

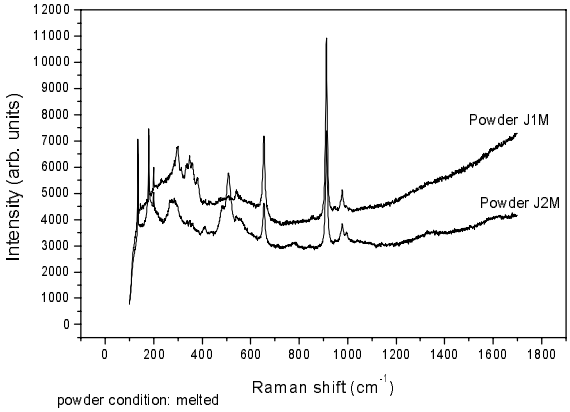

Figure 16 – Raman of powder J (melted)

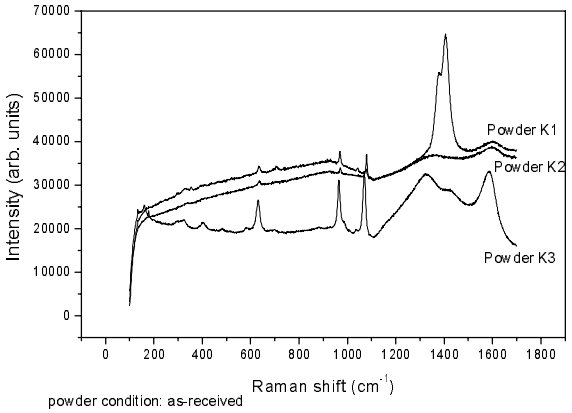

Figure 17 – Raman of powder K (as-received)

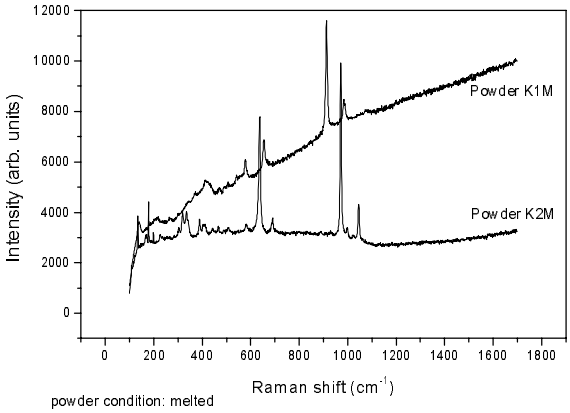

Figure 18 – Raman of powder K (melted)

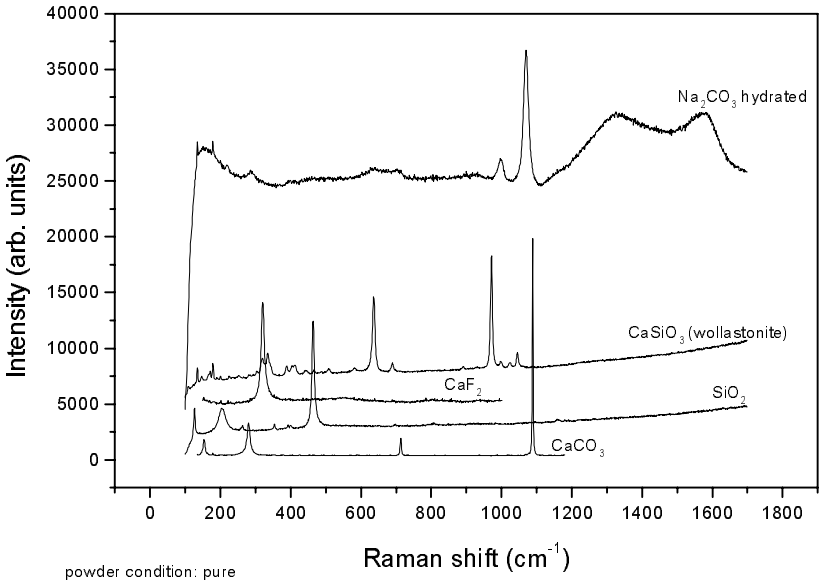

Figure 19 – Raman of the pure phases present in powders I, J and K

7. Presentation of XRD Results for the pure phases presented in the powders.

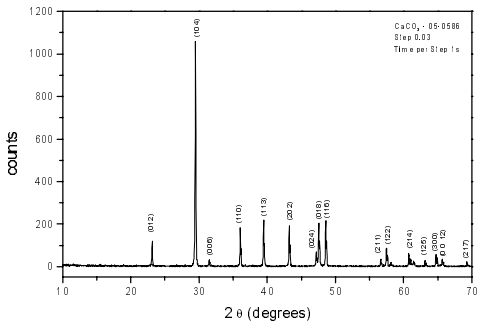

Fig. 20 – XRD of Pure $CaCO_3$

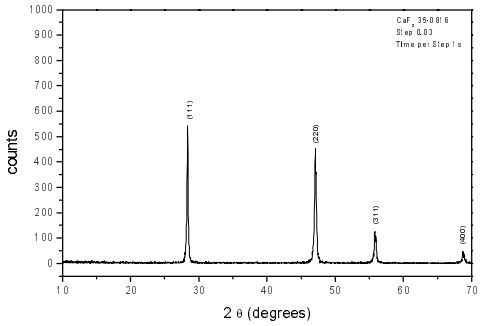

Fig. 21 - XRD of Pure CaF_2

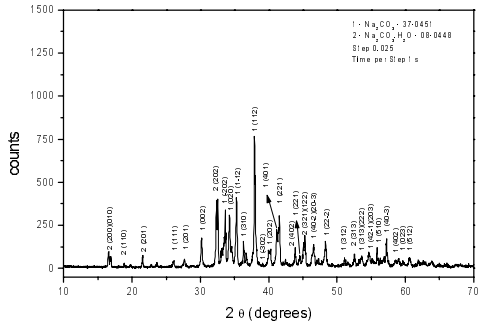

Fig. 22 – XRD of pure and hydrated Na_2CO_3

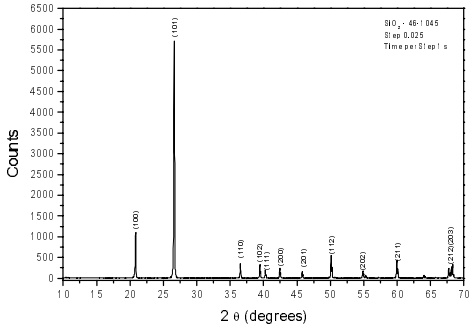

Fig. 23 - XRD of Pure SiO_2

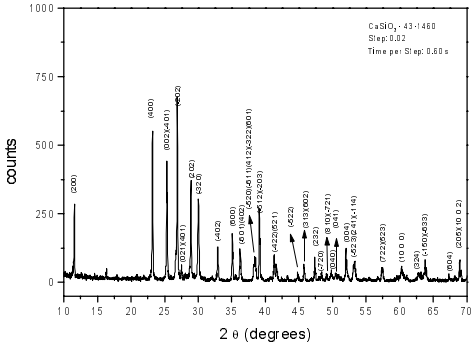

Fig. 24 - XRD of Pure $CaSiO_3$

8. Presentation of thermogravimetric analysis

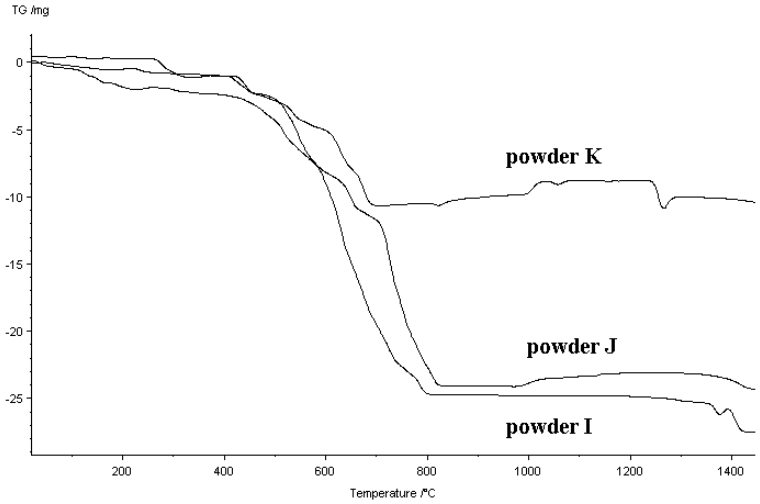

Figure 25 – Thermogravimetric graphic (TG of powders I, J and K)